JOURNAL OF SPACECRAFT AND ROCKETS
Vol. 44, No. 2, March–April 2007

Erratum

Erratum on Low-Density Aerodynamics for the Inflatable Reentry Vehicle Experiment

James N. Moss,* Christopher E. Glass,† and Brian R. Hollis‡
NASA Langley Research Center, Hampton, Virginia 23681-2199
and
John W. Van Norman§
Analytical Mechanics Associates, Inc., Hampton, Virginia 23666-1568

DOI: 10.2514/1.30728
[*J. Spacecraft*, 43(6), pp. 1191–1201 (2006)]

This paper, published in the November–December 2006 issue of *the Journal of Spacecraft and Rockets,* included a number of figures in black and white that should have published in color. The paper is reproduced here in full with the color figures. AIAA regrets the error.

The supersonic transitional flow aerodynamics of the inflatable reentry vehicle experiment are simulated with the direct simulation Monte Carlo method. Also, results from Navier–Stokes calculations are presented that provide both a check on the direct simulation Monte Carlo results near continuum conditions and the general trend of the aerodynamic data at lower altitude conditions. Calculations of axial, normal, and static pitching coefficients are obtained for an angle-of-attack range of 0 to 180 deg. These results clearly demonstrate the strong sensitivity of the aerodynamic coefficients to the relatively low speeds encountered as the inflatable reentry vehicle experiment reenters the atmosphere, and that existing hypersonic aerodynamic data bases for similar geometric configurations are not appropriate for the inflatable reentry vehicle experiment environment. The current numerical simulations focus on the rigid body aerodynamics from 150 to 91 km altitude for the 0 to 180 deg angle of incidence sweep and to lower altitudes (46 km) while at zero incidence.

Nomenclature

A_{ref}	=	reference area, $\pi D^2/4$, m^2
C_A	=	axial coefficient, axial force/$[(0.5\rho_\infty V_\infty^2)(A_{\text{ref}})]$
$C_{m,cg}$	=	pitching-moment coefficient, moment about cg/$[(0.5\rho_\infty V_\infty^2)(A_{\text{ref}})(D)]$
$C_{m,0}$	=	pitching-moment coefficient, moment about nose/$[(0.5\rho_\infty V_\infty^2)(A_{\text{ref}})(D)]$
C_N	=	normal coefficient, normal force/$[(0.5\rho_\infty V_\infty^2)(A_{\text{ref}})]$
D	=	maximum diameter of spacecraft, m
$Kn_{\infty,D,HS}$	=	freestream hard sphere Knudsen number, λ_∞/D
mcs	=	mean collision separation distance, m
mfp	=	mean free path, m
n	=	number density, m^{-3}
p	=	pressure, N/m^2
q	=	wall heat transfer rate, W/m^2
T	=	temperature, K
V_∞	=	freestream velocity, m/s
x, y, z	=	model coordinates, m
X	=	mole fractions
α	=	angle of incidence, deg
λ_∞	=	mean free path in freestream, m
ρ_∞	=	freestream density, kg/m^3

Subscripts

D	=	maximum spacecraft diameter
HS	=	hard sphere
W	=	wall
∞	=	freestream

I. Introduction

THE potential benefits of inflatable decelerators for aerocapture is such that they have generated renewed interest in addressing a number of technical challenges associated with their implementation. If these technologies can be validated, then the inflatables will surpass [1–3] the capabilities of rigid aeroshells in several respects as follows: increased payload mass and volume fraction, postlaunch vehicle integration payload access, use of mission systems during both the in-transit phase and the entry, descent and landing phases, access to higher altitude landing sites upon entry, and provide a more benign payload thermal environment during entry. Included in the family of aerocapture inflatable decelerators [4] (Fig. 1) are trailing ballutes, afterbody attached ballutes, and forebody-attached inflatable aeroshells. This paper focuses on the last configuration, which will be used in the inflatable reentry vehicle experiment (IRVE) [1–3], described pictorially in Figs. 2–4. This flight experiment will be conducted by the NASA Langley Research Center and the NASA Wallops Flight Facility. The current paper describes the methods and procedures used for developing the high altitude aerodynamic data base for IRVE and the implications of the supersonic velocities encountered during reentry.

IRVE is scheduled to be launched from NASA's Wallops Flight Facility by using a Terrier/Orion sounding rocket in March 2007. IRVE represents a first step in an incremental development program for inflatable aeroshell systems. Even though IRVE does not provide a match for interplanetary entry conditions or vehicle size due to the current launch performance and payload volume, IRVE will provide an opportunity to obtain a wealth of data that will contribute significantly to the understanding and the advancement of technology for inflatable decelerators. The IRVE mission and objectives [2] will include demonstration of aeroshell packaging efficiency, materials performance, and methods of construction, inflation, leak performance, structural integrity and aerodynamic stability of the inflatable system, and a trove of data through inertial, radar tracking, photographic, and skin and in-depth temperature measurements. In addition to demonstrating the inflatable aeroshell technology, IRVE will serve [1] to validate structural, aerothermal, and trajectory modeling techniques for inflatables.

The current numerical simulations have been generated with direct simulation Monte Carlo (DSMC) and Navier–Stokes codes, with the major effort focusing on the transitional flow regime by applying the

Presented as Paper 1189 at the 44th AIAA Aerospace Sciences Meeting and Exhibit, Reno, NV, 9–12 January 2006; received 24 January 2006; revision received 17 March 2006; accepted for publication 22 March 2006.

*Senior Research Engineer, Aerothermodynamics Branch, Mail Stop 408A; j.n.moss@larc.nasa.gov. Fellow AIAA.
†Senior Research Engineer, Aerothermodynamics Branch, Mail Stop 408A; c.e.glass@larc.nasa.gov. Senior Member AIAA.
‡Senior Research Engineer, Aerothermodynamics Branch, Mail Stop 408A; b.r.hollis@larc.nasa.gov. Senior Member AIAA.
§Project Engineer, Systems Engineering Branch, Mail Stop 489; j.w.vannorman@larc.nasa.gov.

Fig. 1 Inflatable decelerators for aerocapture, from [4].

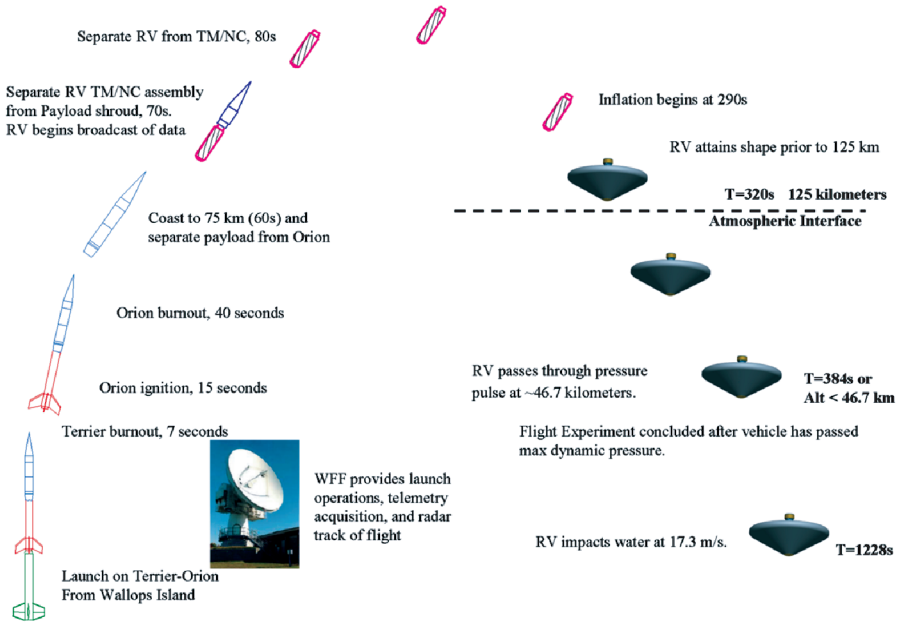

Fig. 2 IRVE concept of operations, from [3].

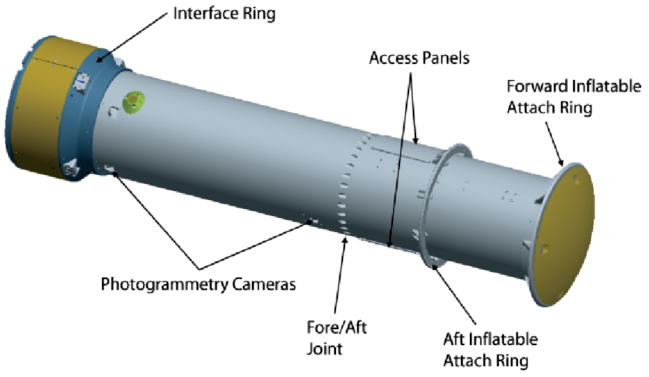

Fig. 3 Centerbody structure with inflatable removed for clarity, from [2].

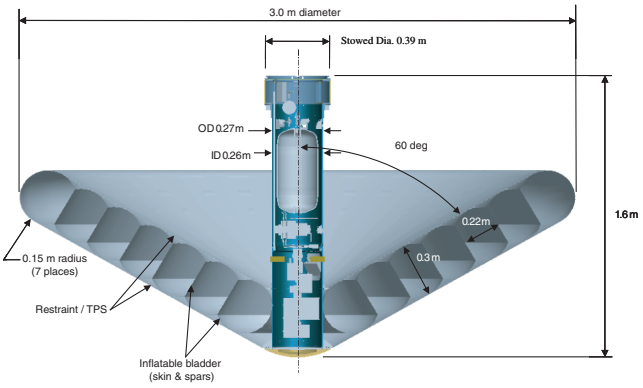

Fig. 4 Cross sectional view of IRVE, from [3].

3-D DSMC codes called DS3V [5,6][‖] and DAC [7] (DSMC analysis code). The Navier–Stokes code that was used is called LAURA [8–10] (Langley aerothermodynamic upwind relaxation algorithm), with results obtained by using both the thin-layer and full Navier–Stokes options. The aerodynamic forces, moments, and the corresponding coefficients are presented for altitudes of 150 km (approximate altitude for complete aeroshell inflation) to 46 km: that is, conditions spanning the flow environment from approximately free molecular, transitional, and much of the continuum regimes. Results of the numerical simulations show a very strong sensitivity of IRVE's aerodynamics to velocity; consequently, IRVE's aerodynamics are substantially different from the data for similar configurations under hypersonic conditions. Results for the static moment coefficients about the center of gravity show that IRVE has a single stable trim point (facing forward) for free molecular conditions, but experiences multiple stable trim points (both forward and backward) for much of the transitional flow regime. Trends evident in the current results indicate that the dual trim situation extends well into the continuum regime. Values for the surface heating show that the maximum stagnation-point heating rates, for zero incidence, are 0.79 W/cm^2 or less, with larger values occurring in the toroidal region or cylindrical centerbody for angles of incidence. Consistency of the DSMC results are demonstrated by the good agreement of results from independent solutions with different codes and by good overall agreement between DSMC and Navier–Stokes (NS) results for similar flow conditions at a Knudsen number of approximately 0.01.

[‖]See http://gab.com.au [cited 15 March 2005].

II. Inflatable Reentry Vehicle Experiment Flight Overview, Configuration, Trajectory, and Flight Conditions

Figures 2–6 provide information concerning the operational aspects (Fig. 2) of the flight experiment, details concerning the physical features and size of IRVE (Figs. 3 and 4), the surface grid (Fig. 5) used to model IRVE's geometry, and information regarding the trajectory parameters (Fig. 6) for which the calculations were made. Tables 1 and 2 list the specific trajectory points selected for analysis.

The operational aspects of the flight experiment depicted in Fig. 2 represent that of a more recent trajectory than that used in the current study; consequently, the time and altitude events are slightly different from that of the current study. For example, the present simulations are made for a trajectory[¶] in which the reentry vehicle (RV) separation from the booster occurs at 64 s and 77.6 km, reaches a maximum altitude of 169.2 km at 204.2 s at a speed of 223 m/s, inflation is initiated at 250 s and 160 km, and the inflation is completed at 270 s and 150 km. When the RV separates from the booster, the RV configuration consists of the centerbody structure shown in Fig. 3, with the stowed inflatable aeroshell folded and packed around the centerbody structure and held in place with a fabric bag. The forward end of the centerbody has a Teflon spherical cap segment attached that forms part of the outer mold line of the spherically blunted cone forebody. The IRVE configuration with the inflated aeroshell and centerbody is displayed in Fig. 4, with its maximum diameter of 3 m. The outer mold line representation of IRVE as implemented in the current study is presented in Fig. 5.

As shown in Fig. 7, the peak heating for the current trajectory occurs at 56 km and the peak dynamic pressure occurs at 46 km, the last point listed in Table 1. Consequently, the maximum aerothermal loads for IRVE occur well into the continuum regime at supersonic conditions, where the density is much higher than what would be experienced for atmospheric aerocapture applications.

The freestream Knudsen numbers are also included in Table 2, where the characteristic length has been chosen as IRVE's maximum diameter (3 m), and the mean free path is evaluated using a hard sphere model with a diameter equal 3.78×10^{-10} m. Values for the freestream hard sphere Knudsen numbers ($Kn_{\infty,D,H,S}$) are listed for data correlation purposes, rather than the variable hard sphere values. Figure 6 presents the velocity and altitude history for a portion of IRVE's trajectory and identifies the time intervals for which DSMC and NS analyses have been applied. Tables 1 and 2 list the trajectory freestream conditions along with the gas composition and molecular

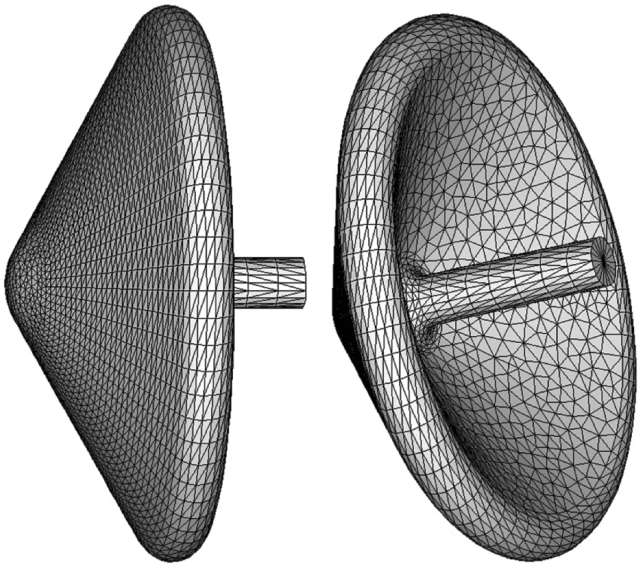

Fig. 5 Views of IRVE unstructured body grid used in present DSMC simulations.

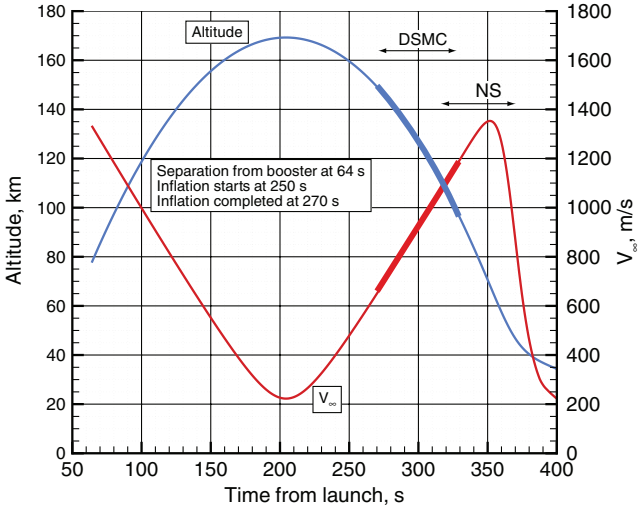

Fig. 6 Velocity and altitude as a function of time.

Table 1 Freestream conditions

Time, s	Altitude, km	V_∞ m/s	n_∞, m^{-3}	ρ_∞, kg/m^3	T_∞, K	Molecular weight
269.2	150	643	5.2253×10^{16}	2.1061×10^{-9}	633	24.273
290.2	135	830	1.3057×10^{17}	5.4480×10^{-9}	517	25.127
302.0	125	937	3.0192×10^{17}	1.2949×10^{-8}	417	25.783
307.0	120	983	4.9348×10^{17}	2.1435×10^{-8}	363	26.159
310.0	117	1011	7.0305×10^{17}	3.0810×10^{-8}	329	26.393
312.0	115	1029	9.1499×10^{17}	4.0455×10^{-8}	305	26.626
315.0	112	1057	1.4424×10^{18}	6.4495×10^{-8}	268	26.929
317.0	110	1075	2.0417×10^{18}	9.2321×10^{-8}	243	27.232
319.0	108	1094	2.9431×10^{18}	1.3434×10^{-7}	224	27.490
322.0	105	1122	5.0947×10^{18}	2.3640×10^{-7}	208	27.943
326.0	100	1159	1.1041×10^{19}	5.1805×10^{-7}	196	28.258
331.0	95	1205	3.1167×10^{19}	1.4835×10^{-6}	188	28.613
——[a]	91	1301	5.0182×10^{19}	2.4048×10^{-6}	185	28.860
338.8	85	1276	1.6665×10^{20}	8.0151×10^{-6}	188	28.964
346.8	75	1337	8.4845×10^{20}	4.0807×10^{-5}	209	28.964
353.8	65	1349	3.1543×10^{21}	1.5171×10^{-4}	232	28.964
360.8	56	1245	9.8736×10^{21}	4.7489×10^{-4}	257	28.964
370.8	46	831	3.5298×10^{22}	1.6977×10^{-3}	267	28.964

[a]Conditions for 3-D LAURA calculations: different trajectory.

[¶]Starr, B. R., private communication, May 2005.

Table 2 Atmospheric composition and Knudsen number for reentry conditions

Altitude, km	X_{O2}	X_{N2}	X_O	$Kn_{\infty,D,HS}$
150	0.05461	0.61557	0.32982	10.05
135	0.06593	0.67158	0.26248	4.02
125	0.07679	0.71171	0.21150	1.74
120	0.08451	0.73271	0.18278	1.064
117	0.09115	0.74328	0.16556	0.747
115	0.09779	0.75386	0.14835	0.574
112	0.11051	0.76214	0.12735	0.364
110	0.12323	0.77042	0.10635	0.257
108	0.13567	0.77531	0.08902	0.178
105	0.15808	0.78319	0.05873	0.103
100	0.17682	0.78440	0.03877	0.0476
95	0.20040	0.78687	0.01273	0.0168
91	0.21303	0.78697	0.0000	0.0104
85	0.2372	0.7628	0.0000	3.15×10^{-3}
75	0.2372	0.7628	0.0000	6.18×10^{-4}
65	0.2372	0.7628	0.0000	1.66×10^{-4}
56	0.2372	0.7628	0.0000	5.32×10^{-5}
46	0.2372	0.7628	0.0000	1.49×10^{-5}

weight taken from Jacchia [11] for an exospheric temperature of 1200 K.

III. Numerical Programs and Model Parameters

A. DSMC Analyses

For the more rarefied flow conditions, two DSMC codes, DS3V and DAC, were used to both generate the data and provide a check on the consistency of the results. The majority of these calculations were made with the DS3V program of Bird [5,6], a general 3-D code that provides both time accurate unsteady flow and time-averaged steady flow simulations. Currently, only a scalar version of this program exists, and all the present simulations were made by using a 3.2 GHz personal computer with a memory of 2.0 GB. The DAC program of LeBeau [7] provides both scalar and parallel processing options. Parallel processing is accomplished by domain decomposition and the parallel version of DAC is employed in the current study. For both DSMC programs, the molecular collisions are simulated with the variable hard sphere molecular model. The Larsen–Borgnakke statistical model [12] controls the energy exchange between kinetic and internal modes. For the present study, the simulations are performed by using a three-species nonreacting air gas model while considering energy exchange between translational, rotational, and vibrational modes. The molecular gas constants used in the current study are those given in [5]. Also, a rotational relaxation collision number of 5 and a temperature dependent vibrational collision number (Eq. 6.53 of [5]) were used. More details regarding the DS3V code can be found in [6], and examples of recent validation studies are presented in [13,14]. Examples of validation studies for the DAC code are given in [15,16] and additional details can be found in [17].

For all simulations, the model surface is assumed to be noncatalytic and at a specified wall temperature of 300 K. As for gas-surface interactions, they are assumed to be diffuse, with full energy accommodation.

The geometric size of the computational domain was varied with the degree of rarefaction of the freestream flow, because the influence of the body on the external flow at high Knudsen numbers extends outward a greater distance than is the case for a denser flow. The total number of cells in the computational domain was also a variable. Grid adaptations implemented in the DS3V simulations produced nominally 20 simulated molecules per cell and those for the DAC simulations nominally 10. The total number of simulated molecules ranged from approximately 1 to 10×10^6 for the DS3V simulations and a maximum of 77×10^6 for DAC. For the DAC simulations, nominally 30 (1.8 GHz) processor were used.

An indicator of the resolution achieved in a DS3V simulation is given by the ratio of the mean collision separation between collision partners to the local mean free path (mcs/mfp). For blunt body flows, as considered herein, the average value for this parameter over the computational domain should be much less than 1 to ensure that the local values of (mcs/mfp) are less than 1 adjacent to the surface. For the DAC code, the user can implement a sequence of grid refinements of the two-level Cartesian grid such that the cell size is small in relation to the local mean free path. Both DSMC codes used the same definition for the IRVE surface geometry; that is, an unstructured grid consisting of 1902 points and 3638 triangles while making use of the problem symmetry such that the flow is computed about only half of the vehicle. This surface definition was deemed acceptable after solutions were generated with the full body grid (Fig. 5) with negligible effect, and also after the grid for the centerbody structure and aeroshell afterbody were substantially enriched (3005 points and 5786 triangles), again with negligible change in results.

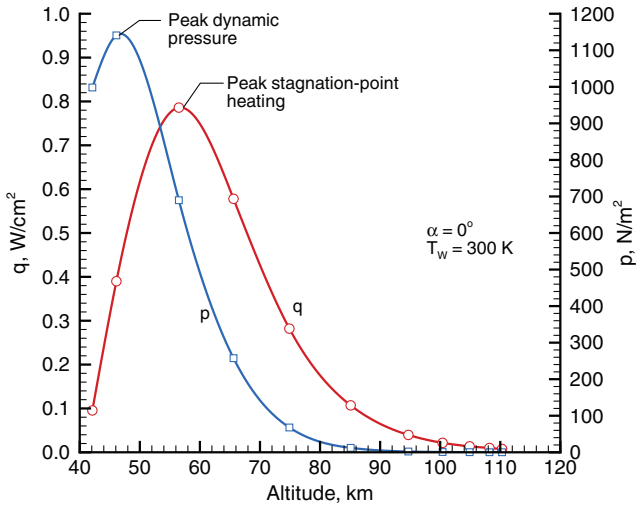

Fig. 7 Stagnation-point heating rate and pressure as a function of altitude-LAURA, full NS results.

B. Navier–Stokes Analyses

Navier–Stokes analyses are performed by using the LAURA computational fluid dynamics code [8–10]. LAURA is an upwind-bias, point-implicit relaxation algorithm for obtaining the numerical solution to the Navier–Stokes equations for three-dimensional, viscous, hypersonic flows in thermochemical nonequilibrium. LAURA has both the thin-layer and full NS options, and both options were exercised in the current study; thin layer for the three-dimensional solutions and both options exercised for the axisymmetric calculations. All of the LAURA simulations assumed the flow to be a perfect gas. For the axisymmetric calculations, the wall temperature was a constant value equal 300 K, and the adapted flowfield grid consisted of 62 points along the IRVE forebody and 96 points out from the surface. For the three-dimensional calculations, a radiative equilibrium wall temperature (surface emissivity of 0.89) was used, the volume grid contained 24 blocks and approximately 334,000 elements, and the computations were made with nominally 24 (2.8 GHz) processors.

IV. Results

Data presented in Figs. 7–25 and Tables 3–7 provide a summary of results for the current study. Context for the IRVE stagnation-point aerothermal loads is depicted in Fig. 7, where the heating rate and pressure results are presented as a function of altitude and where the results have been calculated with the LAURA code by using the full NS option. First, results from the DSMC simulations are discussed where the calculations are for altitudes of 95 to 150 km, the region where the heating rates are small (5% or less) in comparison to the peak heating value, with emphasis on aerodynamics. Near the end of

this section, more details regarding the heating at lower altitudes are presented.

A. Flowfields

Temperature contours and stream traces for two different trajectory points at $\alpha = 0$ deg are presented in Figs. 8 and 9 to illustrate the changing character of the flowfield with rarefaction, 95 and 110 km, respectively. (For the effect of incidence angle on flow features, see Fig. 25 for 95 km results at $\alpha = 75$ deg.) As the freestream density decreases with increasing altitude (an order of magnitude in this example), the shock layer becomes more diffuse and the flow disturbance produced by IRVE is much larger in extent, with the thickness of the merged shock layer equal approximately IRVE's maximum diameter. For both altitudes, the overall kinetic temperature is less than 830 K, indicative of the lack of chemical reactions. Also, the wake flow has well defined vortical features at the 95 km (Fig. 8) condition, but the vortical features are greatly diminished at the 110 km condition and absent at higher altitudes.

B. Aerodynamics Results

Because IRVE does not have an active attitude control system [3], its aerodynamics must provide the capability to align the vehicle to low angles of incidence and damp out oscillations during reentry. When inflated, IRVE's center of gravity (cg) is on the axis of symmetry and located 0.74 m aft of the nose. The current results will show that the static aerodynamics produce a pitching moment about the center of gravity that drives the angle of incidence toward zero for nonzero angles of incidence, provided that the angle of incidence does not exceed 125 deg within the transitional flow regime.

Because IRVE will encounter the transitional flow region at a significant angle of incidence [see Fig. 16, [2], and note that the uninflated (centerbody) configuration is deployed at 180 deg incidence], the manner in which it is able to orient itself in a forward attitude and achieve a relatively small angle of incidence has important implications on the thermal protection system requirements and success of the experiment. As stated in [2], the goal is to keep the stagnation point on the nose during the significant portion of the heating pulse; consequently, during this phase of the entry, the total angle of incidence should not exceed 30 deg and should remain below 30 deg until after peak dynamic pressure.

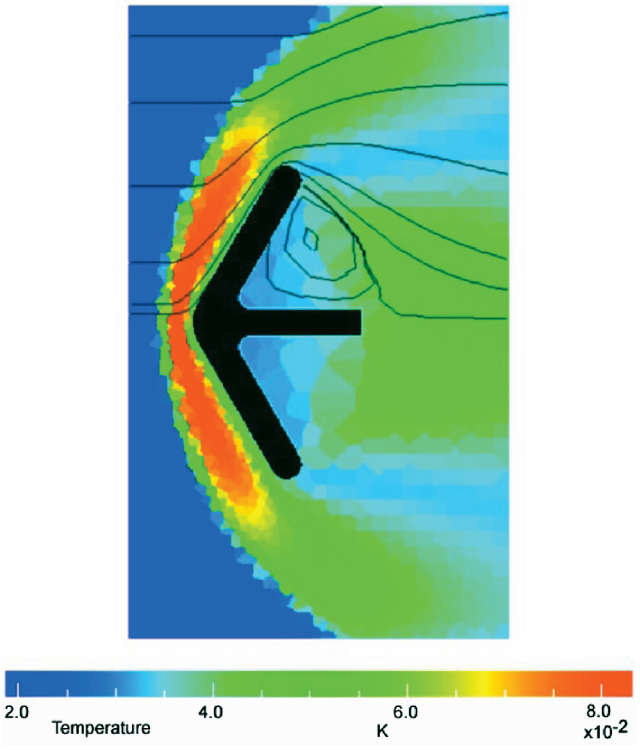

Fig. 8 Temperature contours and stream traces for 95 km and zero incidence: DS3V results.

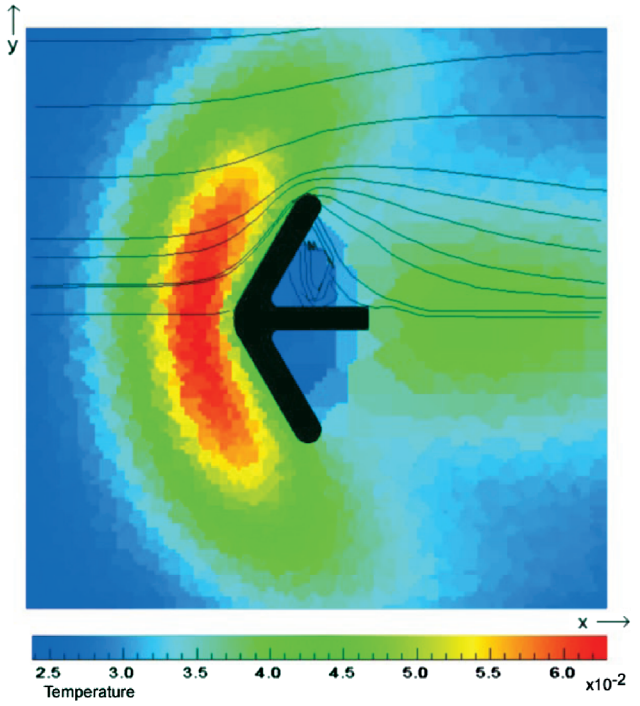

Fig. 9 Temperature contours and stream traces for 110 km and zero incidence: DS3V results.

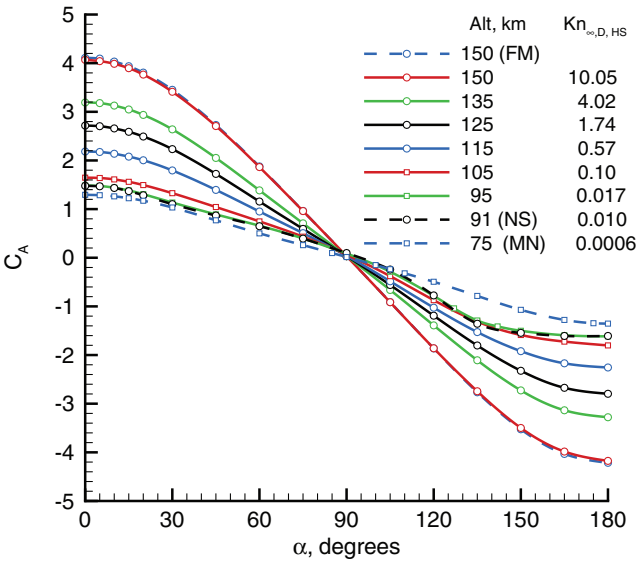

Fig. 10 Calculated axial force coefficients as a function of incidence for selected altitudes (Knudsen numbers).

Representative results of the aerodynamic data generated from the DSMC simulations are included in Tables 3–5, and a more extensive data set is displayed in Figs. 10–14. Data for axial, normal, and moment coefficients are presented, in which the moment data includes that about both the nose and the center of gravity. Results denoted as FM are the free molecular values obtained with the DS3V code for the 150 km altitude flow conditions but with the density reduced by 3 orders of magnitude ($Kn_{\infty,D,H,S} = 10,050$); that is, collisionless flow. The DS3V results show close agreement for the FM and 150 km altitude results. With decreasing rarefaction, the magnitude of the axial (Fig. 10) and normal (Fig. 11) coefficients decrease substantially and the DS3V results at 95 km are shown to be in close agreement with the LAURA thin-layer NS results obtained

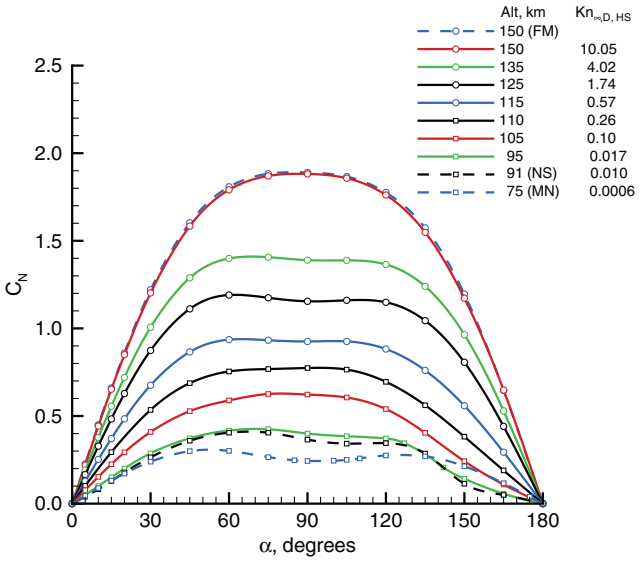

Fig. 11 Calculated normal force coefficients as a function of incidence for selected altitudes.

for a 91 km set of conditions ($Kn_{\infty,D,H,S} = 0.01$), and thereby

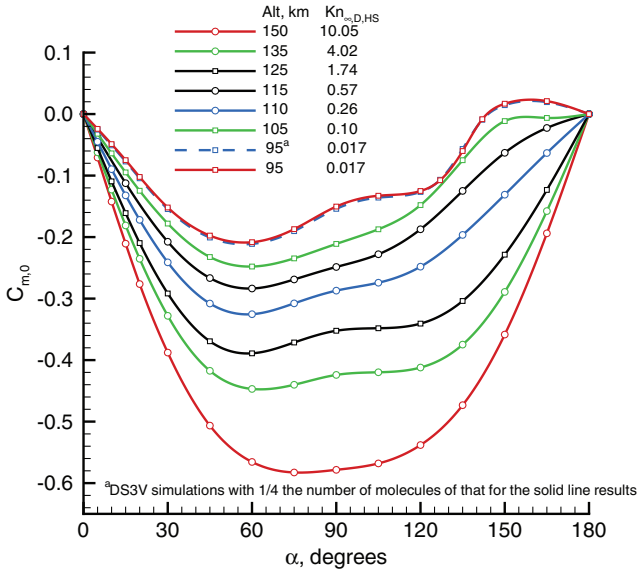

Fig. 12 Calculated moment coefficients (about the nose, $x = 0.0$ with a reference length = 3.0 m).

indicating that the two very different analyses are producing similar results in the 90 to 95 km altitude range.

Only the DS3V results are included in Fig. 12 for the moment coefficients about the nose $C_{m,0}$ in which results are also included that shows the sensitivity of the DS3V simulations to the numerical resolution as expressed by the numerical merit parameter mcs/mfp, the global average of the local cell values of the mean collision separation distance to the local mean free path length. For the 95 km condition, results are included where one set of data was generated with approximately 2.5×10^6 simulated molecules and the second set was generated with approximately 10×10^6 molecules. Table 6 provides additional data that are useful in assessing the goodness of the simulations at the 95 km altitude conditions and for two angles of incidence. As shown in Fig. 12, the $C_{m,0}$ agreement for the 2.5 and 10×10^6 molecule simulations is reasonably good, and the agreement the for other coefficients is equally good.

Results for the moment coefficient about the center of gravity $C_{m,cg}$ are presented in Fig. 13 and an enriched data base in Fig. 14 for the larger angles of incidence where the pitching moment becomes

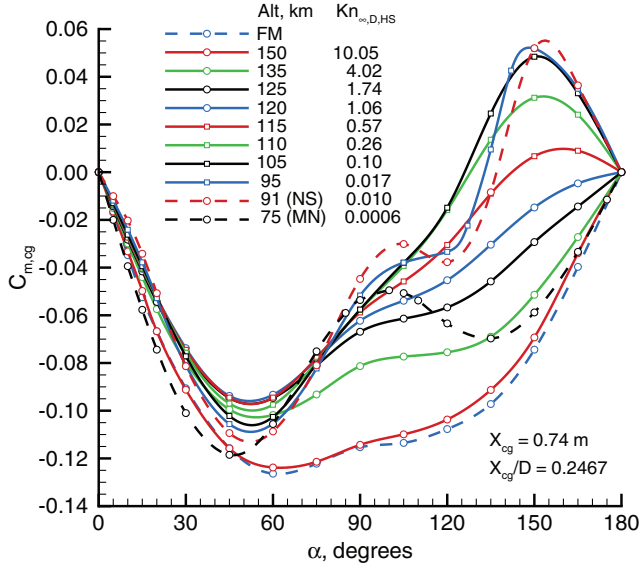

Fig. 13 Calculated moment coefficients about the center of gravity as a function of incidence for selected altitudes.

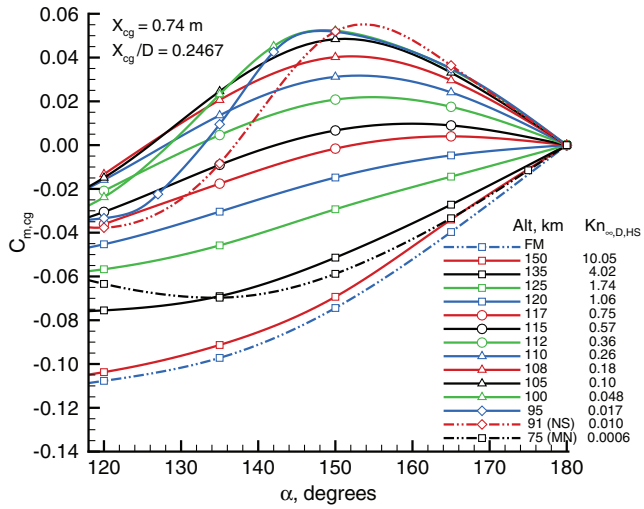

Fig. 14 Enriched data base for moment coefficients at large angles of incidence.

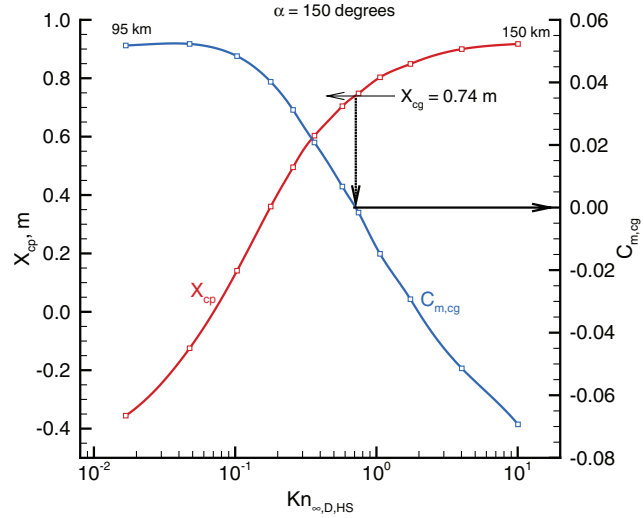

Fig. 15 Sensitivity of center of pressure location and moment coefficient to rarefaction.

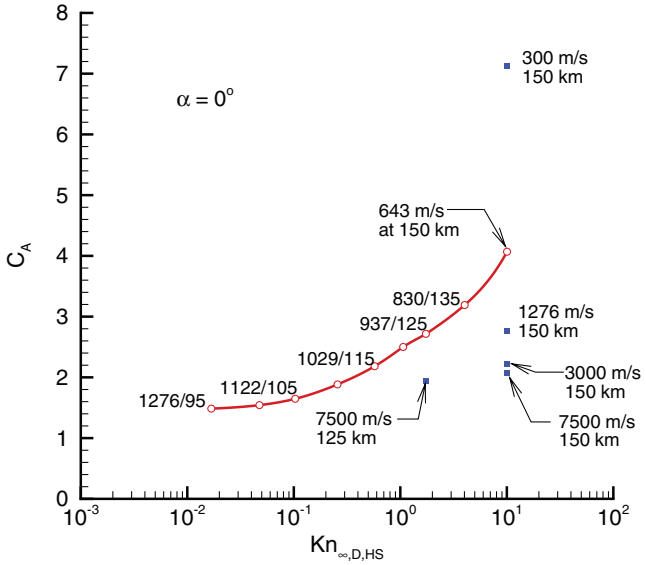

Fig. 16 Sensitivity of calculated axial coefficients to vehicle speed.

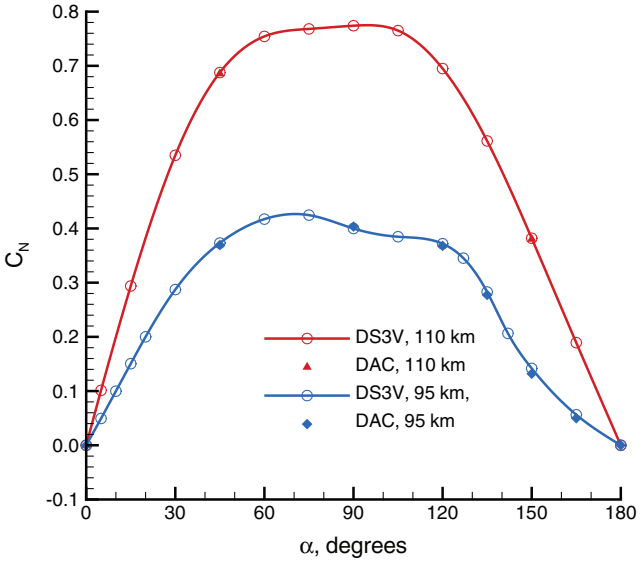

Fig. 19 Comparison of DSMC results for normal force coefficients.

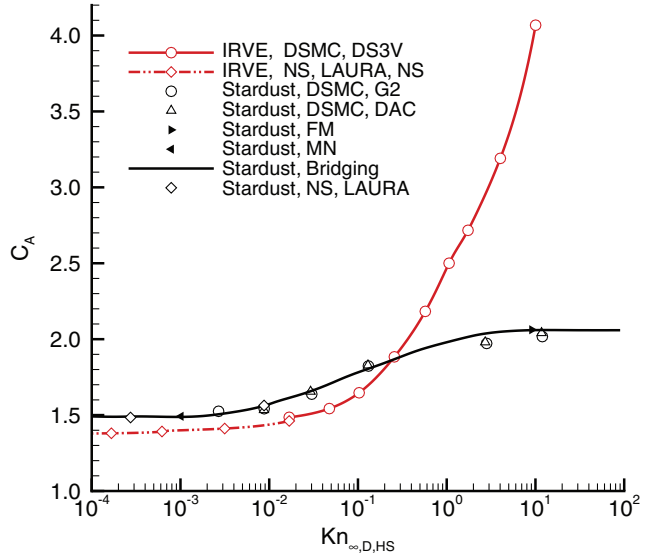

Fig. 17 Axial force coefficients for two 60 deg half angle spherically blunted spacecraft, IRVE and Stardust [18], at zero incidence.

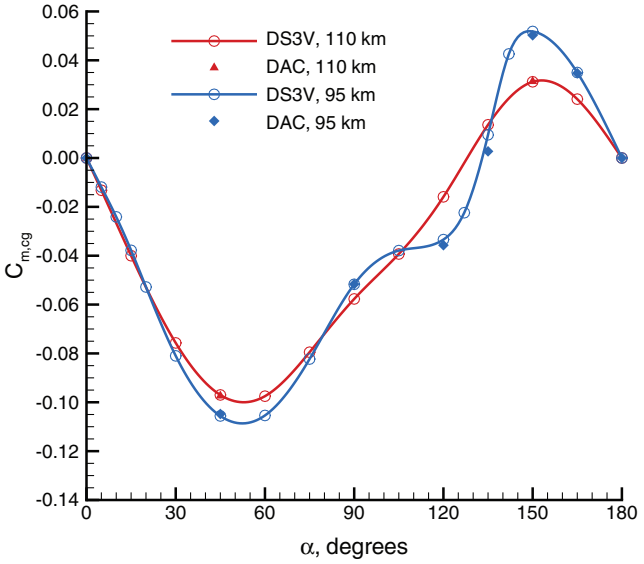

Fig. 20 Comparison of DSMC results for moment coefficients about center of gravity.

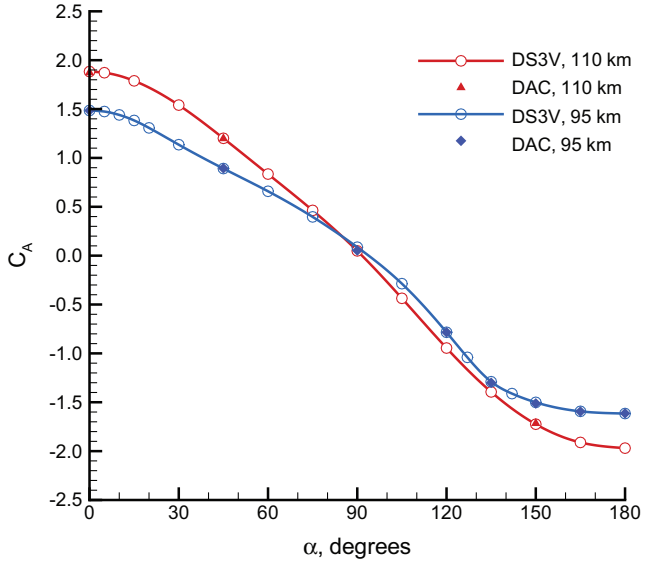

Fig. 18 Comparison of DSMC results for axial force coefficients.

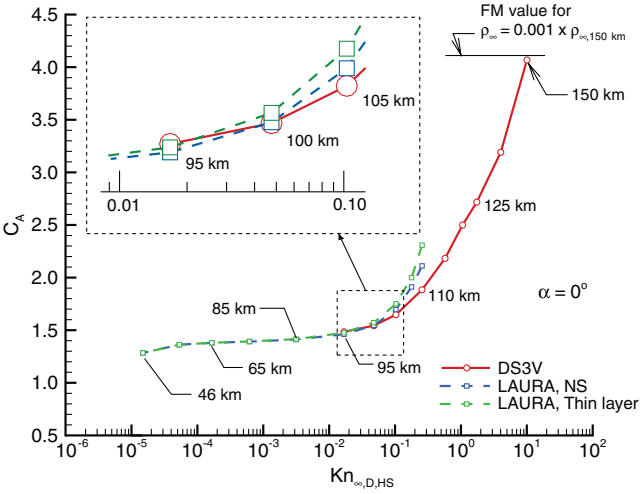

Fig. 21 Calculated axial force coefficients as a function of Knudsen number for zero incidence.

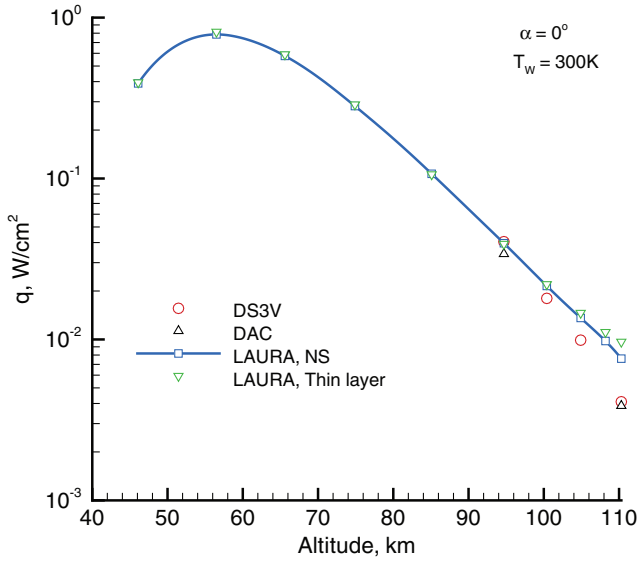

Fig. 22 Stagnation-point heating rate results as a function of altitude.

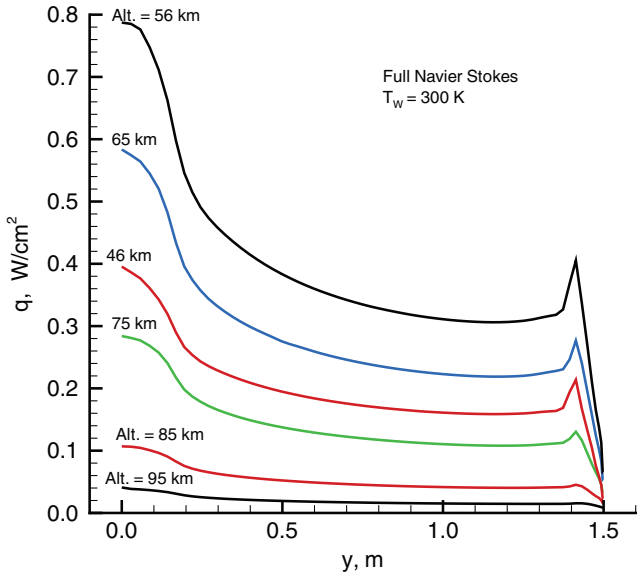

Fig. 23 Heating rate distributions as a function of altitude (LAURA axisymmetric solutions).

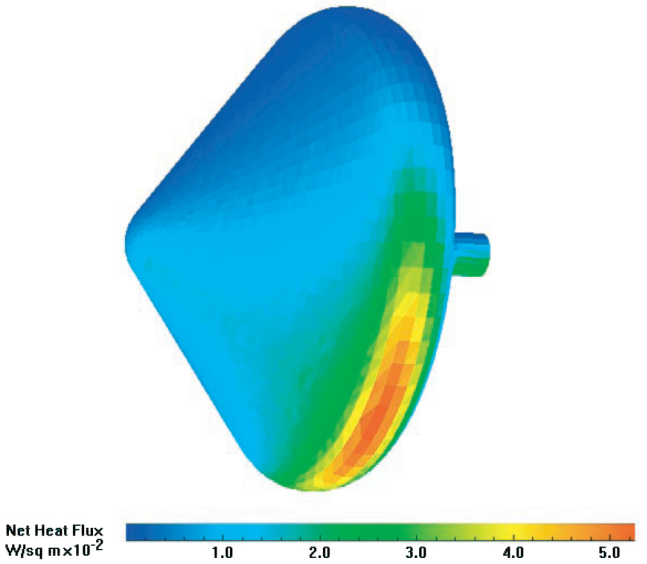

Fig. 24 DS3V surface heating rate results for IRVE at 95 km and 75 deg incidence.

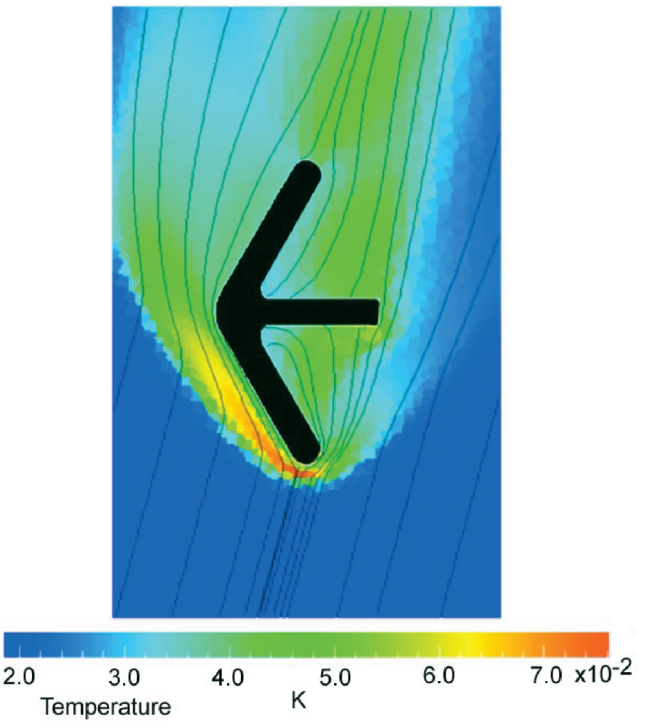

Fig. 25 DS3V results for temperature contours and stream traces at 95 km and 75 deg incidence.

positive and destabilizing. The current results show that IRVE is statically stable with a trim point at $\alpha = 0$ deg for free molecular (FM) conditions and for the more rarefied end of the transitional regime; that is, for Knudsen numbers greater than about 1.0 (altitudes greater than 119 km). For the less rarefied portion of the transitional regime, IRVE has multiple trim angles ($\alpha = 0$ and 180 deg) for altitudes of 118 to 95 km as shown by the DS3V results and also by the LAURA results at 91 km. The data trends are such that the multiple trim points would extend well into the continuum regime, and additional NS calculations would have to be made to determine if and where IRVE returns to a single forward trim situation as is suggested by the modified Newtonian results generated at the 75 km altitude conditions. For reference, the Newtonian results are included in Figs. 10–14. However, the modified Newtonian results are problematic because of the supersonic rather than hypersonic flow conditions and because IRVE has vortical flow features. Furthermore, the modified Newtonian axial force coefficient for the 75 km conditions and zero incidence is 7% less than the LAURA NS results and the agreement between Newtonian and either NS or DSMC becomes progressively worse with increasing altitude.

An indication of the sensitivity of the longitudinal center of pressure location and the resulting moment coefficients to rarefaction are demonstrated in Fig. 15 for an angle of incidence of 150 deg. These data show that the center of pressure x_{cp} moves forward with decreasing rarefaction, crossing the center of gravity at a Knudsen number of 0.67 and continuing the forward movement out in front of IRVE's nose for lower altitudes ($x_{cp} = -0.335$ m at 95 km).

The anticipated attitude behavior of IRVE during flight is discussed in [3], where a Monte Carlo analysis of IRVE's flight simulation is performed with the current aerodynamic data base. Results of this study show that the reentry vehicle attitude is stable exoatmospherically and that the inflated aeroshell aerodynamics is sufficient to align the vehicle to forward flight during reentry. Also,

Table 3 IRVE axial force coefficients C_A as a function of altitude and angle of incidence

Alt., km	$\alpha = 0$ deg	$\alpha = 15$ deg	$\alpha = 30$ deg	$\alpha = 60$ deg	$\alpha = 90$ deg	$\alpha = 120$ deg	$\alpha = 150$ deg	$\alpha = 165$ deg	$\alpha = 180$ deg
FM	4.109	3.937	3.452	1.877	0.0335	−1.864	−3.526	−4.033	−4.215
150	4.068	3.897	3.412	1.864	0.0325	−1.861	−3.499	−3.984	−4.176
135	3.191	3.048	2.640	1.382	0.0327	−1.391	−2.727	−3.135	−3.279
125	2.717	2.589	2.233	1.156	0.0345	−1.191	−2.324	−2.674	−2.796
120	2.500	2.378	2.048	1.058	0.0346	−1.110	−2.138	−2.375	−2.557
117.4	——	——	——	——	——	−1.061	−2.003	−2.402	−2.364
115	2.183	2.079	1.795	0.950	0.0398	−1.026	−1.920	−2.170	−2.256
112.4	——	——	——	——	——	−0.980	−1.802	−2.018	−2.089
110	1.884	1.789	1.540	0.835	0.0487	−0.945	−1.724	−1.911	−1.969
108	——	——	——	——	——	−0.914	−1.659	−1.817	−1.870
105	1.647	1.561	1.328	0.748	0.0631	−0.872	−1.588	−1.724	−1.800
100	1.543	1.450	1.215	0.699	0.0759	−0.829	−1.531	−1.637	−1.667
95	1.485	1.383	1.135	0.659	0.0867	−0.784	−1.501	−1.593	−1.615
95[a]	1.485	——	——	——	0.853	−0.784	−1.512	−1.595	−1.614
91[b]	1.478	1.369	1.102	0.648	0.0973	−0.774	−1.544	−1.608	−1.607

[a]DSMC code DAC.
[b]NS code LAURA for a different trajectory.

Table 4 IRVE normal force coefficients C_N as a function of altitude and angle of incidence

Alt., km	$\alpha = 5$ deg	$\alpha = 15$ deg	$\alpha = 30$ deg	$\alpha = 45$ deg	$\alpha = 60$ deg	$\alpha = 90$ deg	$\alpha = 120$ deg	$\alpha = 150$ deg	$\alpha = 165$ deg
FM	0.226	0.660	1.220	1.603	1.808	1.890	1.779	1.196	0.646
150	0.220	0.652	1.202	1.584	1.791	1.882	1.761	1.172	0.648
135	0.191	0.556	1.006	1.289	1.399	1.390	1.365	0.964	0.529
125	0.166	0.482	0.874	1.112	1.191	1.155	1.149	0.807	0.441
120	0.151	0.440	0.797	1.010	1.082	1.049	1.034	0.705	0.381
117.4	——	——	——	——	——	——	0.945	0.618	0.339
115	0.128	0.372	0.676	0.866	0.936	0.925	0.882	0.559	0.293
112.4	——	——	——	——	——	——	0.772	0.455	0.233
110	0.101	0.294	0.535	0.688	0.754	0.774	0.695	0.382	0.189
108	——	——	——	——	——	——	0.625	0.318	0.150
105	0.0769	0.225	0.409	0.528	0.589	0.622	0.540	0.242	0.109
100	0.0627	0.185	0.341	0.441	0.495	0.512	0.455	0.182	0.0767
95	0.0494	0.150	0.287	0.373	0.417	0.400	0.372	0.142	0.0563
95[a]	——	——	——	0.369	——	0.404	0.368	0.132	0.0498
91[b]	0.0399	0.129	0.265	0.359	0.405	0.365	0.345	0.131	0.0494

[a]DSMC code DAC.
[b]NS code LAURA.

Table 5 IRVE moment coefficients $C_{m,cg}$ as a function of altitude and angle of incidence

Alt., km	$\alpha = 5$ deg	$\alpha = 15$ deg	$\alpha = 30$ deg	$\alpha = 45$ deg	$\alpha = 60$ deg	$\alpha = 90$ deg	$\alpha = 120$ deg	$\alpha = 150$ deg	$\alpha = 165$ deg
FM	−0.0170	−0.0524	−0.0906	−0.1157	−0.1264	−0.1153	−0.1077	−0.0744	−0.0397
150	−0.0165	−0.0498	−0.0912	−0.1158	−0.1238	−0.1143	−0.1037	−0.0693	−0.0340
135	−0.0150	−0.0440	−0.0797	−0.0995	−0.1018	−0.0813	−0.0755	−0.0514	−0.0272
125	−0.0143	−0.0416	−0.0756	−0.0947	−0.0947	−0.0669	−0.0567	−0.0293	−0.0144
120	−0.0137	−0.0405	−0.0738	−0.0938	−0.0933	−0.0623	−0.0453	−0.0148	−0.0047
117.4	——	——	——	——	——	——	−0.0361	0.0016	0.0040
115	−0.0136	−0.0405	−0.0745	−0.0945	−0.0945	−0.0588	−0.0305	0.0067	0.0090
112.4	——	——	——	——	——	——	−0.0209	0.0208	0.0175
110	−0.0132	−0.0400	−0.0757	−0.0970	−0.0975	−0.0577	−0.0159	0.0312	0.0241
108	——	——	——	——	——	——	−0.0133	0.0402	0.0296
105	−0.0130	−0.0394	−0.0772	−0.1022	−0.1026	−0.0576	−0.0149	0.0484	0.0331
100	−0.0124	−0.0382	−0.0783	−0.1036	−0.1044	−0.0557	−0.0238	0.0523	0.0347
95	−0.0119	−0.0378	−0.0810	−0.1056	−0.1054	−0.0517	−0.0334	0.0518	0.0350
95[a]	——	——	——	−0.1048	——	−0.0516	−0.0357	0.0502	0.0347
91[b]	−0.0100	−0.0342	−0.0813	−0.1094	−0.1087	−0.0447	−0.0377	0.0520	0.0364

[a]DSMC code DAC.
[b]NS code LAURA.

this analysis shows ([3], Fig. 21) that the 99.87 percentile maximum angle of incidence is 36 deg at 125 km altitude, but decreases as the vehicle traverses the transitional and continuum regimes such that the maximum value is only 13.5 deg at peak dynamic pressure. That is, the predicted maximum angles of incidence are well below those that would produce a backward trim orientation in the transitional flow regime, based on the results presented in Fig. 13, and falls within the flight experiment's requirement that the angle of incidence remains less than 30 deg from 80 km through maximum dynamic pressure.

C. Sensitivity of Aerodynamics to Velocity

The strong sensitivity of the aerothermodynamic coefficients, particularly at free molecular conditions, to small speed ratio or Mach number conditions is demonstrated in [5] (pp. 162 to 172). This

Table 6 Sensitivity of aerodynamic forces and moments of DS3V simulation merit parameter (mcs/mfp) at 95 km

α, deg	Mean mcs/mfp	Simulated molecules	C_A	C_N	$C_{m,0}$	$C_{m,cg}$
75	1.03	0.544×10^6	0.4046	0.4645	−0.1969	−0.0823
	0.67	2.169×10^6	0.3978	0.4383	−0.1903	−0.0822
	0.43	8.660×10^6	0.3967	0.4249	−0.1872	−0.0824
135	1.23	0.625×10^6	−1.2743	0.3150	−0.0550	0.0227
	0.80	2.488×10^6	−1.2806	0.2956	−0.0570	0.0159
	0.49	9.919×10^6	−1.2898	0.2827	−0.0602	0.0095

Table 7 Axisymmetric LAURA results for axial force coefficient and stagnation-point heating rate and pressure

Quantity	95 km	85 km	75 km	65 km	56 km	46 km
C_A	1.461	1.411	1.392	1.380	1.362	1.284
q, W/cm^2	0.0396	0.107	0.282	0.578	0.786	0.390
p, N/m^2	2.05	12.2	67.8	257	690	1141

sensitivity is also evident in the transitional regime as demonstrated in Fig. 16, where the freestream velocity is arbitrarily altered at two altitudes for the IRVE configuration. For example, if the velocity for the 125 km condition is increased from 0.937 to 7.5 km/s, the axial coefficient becomes 1.942, a small value that is 71% of that for the current lower speed IRVE flight condition. The effect of altering the velocity at 150 km, both increasing and decreasing the velocity relative to that of IRVE, shows that the axial coefficients have a very strong sensitivity to velocity at supersonic and lower speeds.

D. Comparisons of IRVE Data to Hypersonic Data for a Similar Aeroshell Configuration

Because of the strong sensitivity of the aerodynamics to flow velocity, one might suspect that existing hypersonic databases for configurations similar to IRVE would not be appropriate. Comparison of the axial force coefficients for IRVE and the Stardust (Fig. 17) spacecraft, both spherically blunted 60 deg half angle forebodies (different shoulder radii), show this to be the case. The Stardust calculations [18] were made for hypersonic conditions, at reentry velocities of approximately 12.6 km/s.

A second important point made with the data presented in Fig. 17 is that a good overlap or consistency is achieved for the axial force coefficients generated with the DSMC and NS codes, for both IRVE and Stardust applications.

E. Comparisons of Independent DSMC Simulations

Independent calculations conducted with the DAC code served as an additional check on the credibility of the DS3V results, particularly for the lower altitude (95 km) cases investigated with DSMC. DAC simulations were made at two altitudes (110 and 95 km) by using the same surface grid definition as was used in the DS3V simulations. Comparisons of the DS3V and DAC results are presented in Figs. 18–20 for axial, normal, and moment coefficients, respectively. As demonstrated by the results, the agreement between the two simulations is very good. For the DAC simulations, the number of simulated molecules were on the order of 70×10^6, almost an order of magnitude grater than that used in the DS3V simulations. Tabulated results for the DAC simulations at 95 km are included in Tables 3–5. The DAC data for the 110 km cases are not included because it was essentially the same as the DS3V results, which is more extensive and is tabulated.

F. Aerodynamics in the Rarefied and Continuum Regimes

Figure 21 provides a summary of the axial or drag coefficients as a function of Knudsen number that spans IRVE's reentry trajectory from free molecular through peak heating and to the point of peak dynamic pressure (46 km altitude). (See Table 7 for a listing of the aerodynamic results from the axisymmetric LAURA calculations.) Shown are the DS3V and LAURA solutions for zero incidence. As mentioned earlier, these are the LAURA axisymmetric results and the simulations accounted for only the forebody and the no slip, no temperature jump boundary conditions were used. The LAURA solutions were made by using both the thin-layer and full NS options, and the axial force coefficients are similar for the higher density conditions, where one has a thin layer, but begins to differ at the higher altitudes where the shock layer becomes much thicker, with the ultimate merger of the boundary layer and bow shock. Overlap of the DSMC and the full NS results is shown to be good in the altitude range of 95 to 100 km (Knudsen numbers up to 0.05), but poor at 105 km and higher.

G. Aerodynamic Heating

As previously shown in Fig. 7, the heating for IRVE is only significant in the continuum regime when referenced to the peak heating value. The differences observed in the NS and DSMC stagnation-point heating values for zero incidence are presented in Fig. 22. At 95 km, the LAURA full NS and DSMC solutions are in good agreement, but the LAURA results with increasing altitude yields values that are substantially higher than the results provided by the DSMC codes. As for the nature of the forebody surface distributions at zero incidence, Fig. 23 presents heating rate distributions for altitudes between 95 and 46 km.

When IRVE is at an angle of incidence, the maximum heating can be substantially higher than the corresponding zero incidence, stagnation-point value. This is demonstrated for IRVE at 95 km and $\alpha = 75$ deg in Fig. 24, where the surface heating rate contours are presented for a DS3V simulation and the corresponding flowfield temperature contours and stream traces are presented in Fig. 25. For this case the peak heating (0.052 W/cm^2) is 27% higher than the corresponding stagnation-point value for $\alpha = 0$ deg. One additional example is for IRVE at 95 km and $\alpha = 135$ deg where the peak heating occurs on the centerbody with a value of 0.060, or 46% higher than the stagnation-point value for $\alpha = 0$ deg. These examples of enhanced heating rates due to vehicle attitude are indicative of the more serious issues of high angles of incidence excursions in the continuum regime.

V. Conclusions

A computational study of supersonic flow over IRVE is made by using the direct simulation Monte Carlo (DSMC) and Navier–Stokes (NS) codes to provide aerodynamic forces, moments, and heating information. Results of the numerical simulations show that the NS method with the no slip and no temperature jump surface boundary conditions provide results that are in close agreement with that from DSMC for altitudes between 90 and 95 km, or a hard sphere Knudsen number of about 0.01. A major focus of the current study is to provide

an aerodynamic data base for IRVE in the transitional to free molecular regime; the regime where the surface heating rates are small to negligible with respect to peak heating. For the IRVE trajectory analyzed, inflation occurs near 150 km, and aerodynamic data have been generated using DSMC for several altitudes between 150 and 95 km for angle of incidence sweeps of 0 to 180 deg. The same information has been generated with NS for only one altitude (91 km). In addition, axisymmetric NS simulations were made for the forebody of IRVE that provide insight into the aerodynamic forces and heating for an altitude span of 110 to 46 km. These axisymmetric calculations include both the peak heating and the peak dynamic pressure points along the trajectory. The higher altitude results (above 95 km) clearly demonstrate, in a quantitative manner, the shortcomings of the NS approach for the more rarefied regime where the NS-predicted heating and axial forces become progressively larger than those predicted by DSMC. Also, results are presented that demonstrate the sensitivity of NS results to the use of either the full NS formulation or the thin-layer version; with the latter formulation providing noticeably poorer results for the more rarefied conditions.

Significant findings of the present investigation are as follows: 1) a very strong sensitivity of the aerodynamics to velocity is demonstrated; 2) aerodynamic data bases for similar configurations at hypersonic conditions are not appropriate for the conditions that IRVE will experience; 3) IRVE is statically stable at free molecular conditions (a single stable trim point at zero incidence) but exhibits multiple stable trim points (0 and 180 deg incidence) for much of the transitional flow regime and the data suggest that the situation persists well into the continuum regime; 4) additional NS results are necessary to clarify where and if IRVE exhibits a single forward trim point in the continuum regime; 5) for angles of incidence, local surface heating rates can be significantly higher on either the inflated aeroshell or the center body structure than that experience at the stagnation point for zero incidence; and 6) the consistency of the DSMC results is demonstrated by the good agreement shown for independent solutions when using different codes.

Acknowledgments

The authors acknowledge the assistance of the following individuals: Victor Lessard of Genex Systems for providing the unstructured surface grid, Brett R. Starr and Neil Cheatwood of the NASA Langley Research Center for providing the trajectory data and guidance in developing the IRVE aerodynamic database, respectively, and Richard Wheless of NCI Information Systems for assisting with the graphics.

References

[1] Player, C. J., Cheatwood, F. M., and Corliss, J., "Development of Inflatable Entry Systems Technologies," *Proceedings of the 3rd International Planetary Probe Workshop*, 2005.

[2] Hughes, S. J., Dillman, R. A., Starr, B. R., Stephan, R. A., Lindell, M. C., Player, C. J., and Cheatwood, F. M., "Inflatable Reentry Vehicle Experiment (IRVE) Design Overview," AIAA Paper 2005-1636, May 2005.

[3] Starr, B. R., Bose, D. M., Thornblom, M., and Kilcoyne, D., "Inflatable Reentry Vehicle Experiment Flight Performance Simulations," *Proceedings of the 53rd JANNAF Propulsion Meeting*, 2005.

[4] Buck, G. M., "Testing of Flexible Ballutes in Hypersonic Wind Tunnels for Planetary Aerocapture," AIAA Paper 2006-1319, Jan. 2006.

[5] Bird, G. A., *Molecular Gas Dynamics and the Direct Simulation of Gas Flows*, Clarendon Press, Oxford, 1994.

[6] Bird, G. A., "Visual DSMC Program for Three-Dimensional Flows," *The DS3V Program User's Guide, Version 1.2*, March_2005.

[7] LeBeau, G. J., "A Parallel Implementation of the Direct Simulation Monte Carlo Method," *Computer Methods in Applied Mechanics and Engineering, Parallel Computational Methods for Flow Simulation and Modeling*, Vol. 174, 1999, pp. 319–337.

[8] Gnoffo, P. A., "An Upwind-Biased, Point-Implicit Algorithm for Viscous, Compressible Perfect-Gas Flows," NASA TP-2953, Feb. 1990.

[9] Gnoffo, P. A., Gupta, R. N., and Shinn, J. L., "Equations and Physical Models for Hypersonic Air Flows in Thermal and Chemical Nonequilibrium," NASA TP-2867, Feb. 1989.

[10] Cheatwood, F. M., and Gnoffo, P. A., "User's Manual for the Langley Aerothermodynamic Upwind Relaxation Algorithm (LAURA)," NASA TM 4674, April 1996.

[11] Jacchia, L. G., "Thermospheric Temperature, Density, and Composition: New Models," Smithsonian Astrophysical Observatory, Special Rept. 375, Cambridge, MA, March 1977.

[12] Borgnakke, C., and Larsen, P. S., "Statistical Collision Model for Monte Carlo Simulation of Polyatomic Gas Mixture," *Journal of Computational Physics*, Vol. 18, No. 4, 1975, pp. 405–420.

[13] Bird, G. A., "The DS2V/3V Program Suite for DSMC Calculations," *Rarefied Gas Dynamics, 24th International Symposium*, edited by M. Capitelli, Vol. 762, American Institute of Physics, Melville, NY, 2005, pp. 541–546.

[14] Moss, J. N., and Bird, G. A., "Direct Simulation Monte Carlo Simulations of Hypersonic Flows with Shock Interactions," *AIAA Journal*, Vol. 43, No. 12, 2005, pp. 2565–2573; also AIAA Paper 2004-2585, 2004.

[15] Blanchard, R. C., Wilmoth, R. G., and Moss, J. N., "Aerodynamic Flight Measurements and Rarefied-Flow Simulations of Mars Entry Vehicles," *Journal of Spacecraft and Rockets*, Vol. 34, No. 5, 1997, pp. 687–690.

[16] Blanchard, R. C., Wilmoth, R. G., and LeBeau, G. J., "Rarefied-Flow Transition Regime Orbiter Aerodynamic Acceleration Flight Measurements," *Journal of Spacecraft and Rockets*, Vol. 34, No. 1, 1997, pp. 8–15.

[17] LeBeau, G. J., and Lumpkin, F. E., III, "Application Highlights of the DSMC Analysis Code (DAC) Software for Simulating Rarefied Flows," *Computer Methods in Applied Mechanics and Engineering*, Vol. 191, Dec. 2001, pp. 595–609.

[18] Wilmoth, R. G., Mitcheltree, R. A., and Moss, J. N., "Low-Density Aerodynamics of the Stardust Sample Return Capsule," *Journal of Spacecraft and Rockets*, Vol. 36, No. 3, 1999, pp. 436–441.

A. Ketsdever
Associate Editor